



Cite this: *Chem. Commun.*, 2016, 52, 5718

Received 7th December 2015,
Accepted 23rd March 2016

DOI: 10.1039/c5cc10070d

www.rsc.org/chemcomm

Creation of hollow SAPO-34 single crystals via alkaline or acid etching†

Yuyan Qiao,^{ab} Miao Yang,^a Beibei Gao,^{ab} Linying Wang,^a Peng Tian,^{*a} Shutao Xu^a and Zhongmin Liu^{*a}

Hollow SAPO-34 crystals are created via selective etching of their precursor under controlled alkaline or acid conditions. The abundant/interconnected Si–O–Al domains and Si–O–Si networks at the outer layer of SAPO-34 crystals are revealed to be decisive factors for the base and acid treatments respectively to achieve a well-preserved hollow structure.

Hollow materials have attained increasing interest due to their promising applications in catalysis, electronics, medicine, and so on.¹ So far, various types of hollow materials have been prepared including zeolites, carbon, metals, *etc.* Among them, hollow zeolites represent an interesting group because of their unique microporosity which allows an easy access to the interior and provides an ideal shell for shape-selectivity catalysis.²

Direct crystallization is the ideal route to the synthesis of hollow zeolites, which still remains a challenge due to the complexity and variety of synthetic gel chemistry.³ Layer-by-layer assembly, using a hard template as the core and zeolite nanocrystals as the building block, offers a universal way to prepare hollow zeolite spheres.^{2a} However, the hollow products formed with a polycrystalline shell are generally of micrometer size, which limits their use as catalytic nanoreactors. Post-synthetic treatment was first developed by Perez-Ramirez *et al.* in 2005, which provides an alternative approach to obtain hollow-structured zeolites of micro- or nanosizes.⁴ Mesoporosity may develop during alkaline treatment, which would increase the accessibility of the hollow interior and benefit the mass transfer in catalytic reactions.⁵ Since then, many studies on post-processing methods have been carried out, and hollow silicalite-1, ZSM-5 and TS-1 have been successfully prepared.^{5a,6} Compositional zoning and structural defects are generally considered to be the possible

reasons for the generation of hollow single crystals, though the exact mechanism has not been fully understood. It is noted that post-synthetic treatment to fabricate a hollow morphology is hitherto only limited to base leaching and zeolites with the MFI structure.

SAPO molecular sieves are important members of the zeolitic family, which have found applications in industries as heterogeneous catalysts.⁷ In contrast to the success achieved in the preparation of hollow-structured aluminosilicate zeolites, the preparation of hollow SAPO materials, particularly those in a controlled manner, remains a difficult task. And less knowledge exists about the impact of postsynthetic treatment on the morphology and framework composition evolution of SAPOs. This is possibly due to the weaker stability of SAPO frameworks in acidic or basic aqueous solution.⁸

Herein, we demonstrate that hollow SAPO-34 single crystals with good crystallinity can be successfully prepared by controlled acid or base etching. This is the first time that a post-processing route has been employed to tailor the morphology of SAPO molecular sieves. The requirements for the SAPO crystals to form well-preserved hollow structures have been researched, involving framework elemental compositions, atomic coordination environments and distribution in the crystals. The present work not only provides facile strategies to prepare hollow SAPOs, but also offers insights into the stability of local atomic environments of SAPOs in acid and base media.

The SAPO-34 precursor (named as SP34-P) was hydrothermally synthesized by using TEOAH and TMEDA as templates and fully milled SAPO-34 powder as seeds.⁹ Fig. 1 presents the SEM and TEM images of the samples, from which a cube-like morphology with an uneven surface could be observed for SP34-P. Its crystal size is about 400–500 nm. The concrete conditions for base treatment are listed in Table S1 (ESI†). Taking TEOAH as an example, the hollow SAPO-34 product with good crystallinity (Fig. S1, ESI†) is prepared by the treatment of the precursor in 0.6 M TEOAH solution at 180 °C for 1 h. From Fig. 1, the outer surface of SP34-TEAOH crystals is observed to remain relatively intact and no obvious holes can be perceived. The TEM image

^a National Engineering Laboratory for Methanol to Olefins, Dalian National Laboratory for Clean Energy, Dalian Institute of Chemical Physics, Chinese Academy of Sciences, Dalian 116023, P. R. China.
E-mail: tianpeng@dicp.ac.cn, liuzm@dicp.ac.cn

^b University of Chinese Academy of Sciences, Beijing 100049, P. R. China

† Electronic supplementary information (ESI) available. See DOI: 10.1039/c5cc10070d

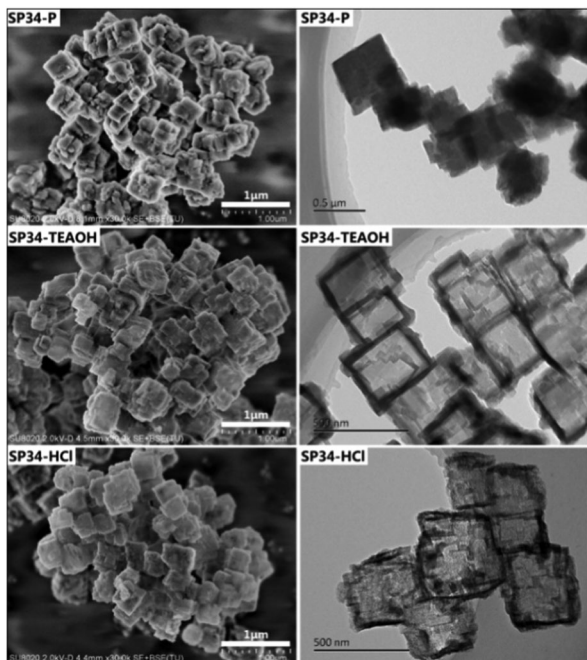


Fig. 1 SEM (left) and TEM (right) images of the samples.

reveals that large voids have been created in the interior of SAPO-34 crystals and the thickness of the shells is about 40 nm. Besides TEOAH, various organic amines (*e.g.* TMAOH, TPAOH, DEA) show the ability to create hollow-structured SAPO-34 (Fig. S2, ESI[†]). Alternatively, when the inorganic base NaOH is employed, a hollow product could also be yielded, but amorphization of SAPO frameworks may occur (Fig. S1 and S3, ESI[†]). The stronger alkalinity of NaOH might extract more framework atoms selectively. The changes of the product compositions will be discussed in the following part. Indeed, inorganic base treatments have been found to amorphize Y and beta zeolites,¹⁰ though NaOH treatment can enable the preparation of mesoporous ZSM-5.¹¹

In addition to base treatment, we also succeeded in preparing hollow SAPO-34 *via* acid etching (Table S1, ESI[†]). It should be mentioned that it is the first time that such morphology has been achieved for zeolitic materials through an acid treatment approach. By employing HCl as the leaching agent, SAPO-34 with a hollow structure and moderate crystallinity is obtained after refluxing in 0.58 M HCl solution at 80 °C for 3 h. Fig. 1 indicates that the crystal size of SP34-HCl is similar to that of SP34-P. The wall thickness is about 30 nm, which is thinner than the base-treated samples and is in agreement with its lower yield. Moreover, the crystal surface of SP34-HCl is a little rough as compared with that of SP34-TEAOH, possibly due to a stronger corrosiveness on the crystal external surface under the acidic conditions. Upon further increasing the temperature to 180 °C, the product (SP34-HCl-i) turns into dense tridymite (amorphous materials may also exist as deduced from the weak XRD peak intensity), though the hollow morphology is still well retained (Fig. S1 and S3, ESI[†]).

Table 1 gives the textural results of the samples determined from N₂ adsorption isotherms (Fig. S4, ESI[†]). The precursor

Table 1 The textural properties of the samples

Sample	Surface area (m ² g ⁻¹)		Pore volume (cm ³ g ⁻¹)	
	S_{BET}^a	S_{ext}^b	V_{micro}^c	V_{total}^d
SP34-P	613	8	0.28	0.31
SP34-TEAOH	614	53	0.26	0.37
SP34-HCl	705	148	0.23	0.49

^a BET surface area. ^b t-plot external surface area. ^c t-plot microporous volume. ^d V_{total} is evaluated at $P/P_0 = 0.99$.

SP34-P has a large microporous surface area and microporous volume. After post-treatment, an obvious increase in the external surface area and total pore volume can be observed, especially for the acid-treated hollow sample SP34-HCl. Because there is only limited development in the mesoporosity of the post-treated samples as deduced from N₂ isotherms, the increased external surface area and pore volume are supposed to be a result of the creation of large voids inside the crystals. Besides, the rough surface of SP34-HCl should also contribute to its largest external surface area (148 m² g⁻¹) and pore volume (0.49 cm³ g⁻¹).

In order to better understand why the etching occurs selectively in the crystal interior, both the surface and bulk compositions of the samples are measured. As given in Table 2, the precursor SP34-P has a Si-rich outer surface, in agreement with our previous findings.¹² After acid or base treatment, the surface Si enrichment degree (*R* value) shows a decrease, although Si enrichment phenomenon still exists. The surface Si content of the treated samples is higher than that of the precursor, implying that the crystal surface is also modified during the hollowing process. For the bulk compositions, the Si content in the hollow products increases evidently, whereas the Al and P contents decrease. The drop of P content in the base-treated samples is greater than that of Al, suggesting the highest sensitivity of P to base leaching. However, the acid treatment results in a greater decrease of Al content than P. This phenomenon is more obvious for SP34-HCl-i from the harsh acid treatment, implying the worst stability of Al among the three framework T atoms. These results suggest that the formation of hollow SAPO morphology may be related to the different chemical stabilities and the inhomogeneous spatial distribution of the framework T atoms in SAPO-34 crystals.

Solid-state MAS NMR spectra are further examined to investigate the local atomic environments in the samples. As shown in Fig. 2, the ²⁹Si spectrum of the precursor SP34-P is complex, in which the five peaks ranging from -91 to -110 ppm correspond to

Table 2 Bulk and surface compositions of the samples

Sample	Product composition		R^a
	Bulk (XRF)	Surface (XPS)	
SP34-P	Si _{0.208} Al _{0.435} P _{0.357}	Si _{0.319} Al _{0.394} P _{0.287}	1.53
SP34-TEAOH	Si _{0.366} Al _{0.390} P _{0.244}	Si _{0.385} Al _{0.359} P _{0.256}	1.05
SP34-NaOH	Si _{0.581} Al _{0.317} P _{0.102}		
SP34-HCl	Si _{0.383} Al _{0.345} P _{0.272}	Si _{0.524} Al _{0.265} P _{0.211}	1.37
SP34-HCl-i	Si _{0.470} Al _{0.265} P _{0.265}		

^a $R = [\text{Si}/(\text{Al} + \text{P} + \text{Si})]_{\text{surface}}/[\text{Si}/(\text{Al} + \text{P} + \text{Si})]_{\text{bulk}}$.

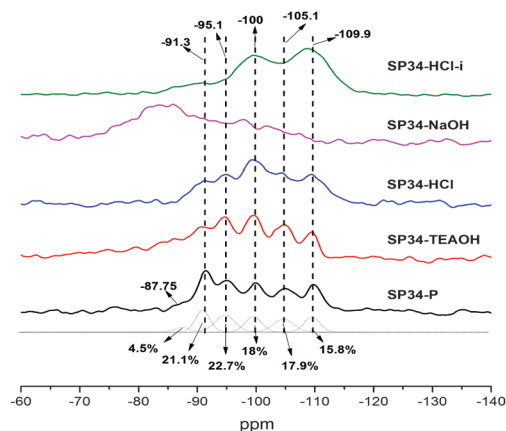


Fig. 2 ^{29}Si MAS NMR spectra of the samples.

$\text{Si}(\text{OSi})_n(\text{OAl})_{(4-n)}$ ($n = 0-4$) species respectively.¹³ In addition, one weak peak around -88 ppm may be discerned, which is attributable to $\text{Si}(\text{OAl})_3(\text{OH})$ or $\text{Si}(\text{OSi})(\text{OAl})(\text{OH})_2$ species at the defective sites. Deconvolution results reveal that the $\text{Si}(\text{OAl})_4$ content only amounts to 21.1% and the five fully condensed Si species are present at close percentages. Such Si environments are rather scarce for SAPO molecular sieves. For the spectrum of SP34-TEAOH, a slight broadness together with variation in the relative peak intensities occurs. The contents of the $\text{Si}(\text{OAl})_4$ and $\text{Si}(\text{OSi})_4$ species drop, whereas the amount of defective Si species shows an increase. In the case of NaOH treatment, the $\text{Si}(\text{OSi})_4$ species in the framework are completely leached. The partially hydrolyzed Si species located in Si–Al environments become dominant as noticed by the broad resonances in the range of -70 to -90 ppm, which is consistent with the amorphous characteristic of SP34-NaOH and indicates that Si–O–Al domains have the best stability in base solution. For the acid-treated sample SP34-HCl, the resonance of around -99 ppm becomes the strongest accompanied by a decrease of the peak at -91 ppm as compared with that of SP34-P. The $^1\text{H} \rightarrow ^{29}\text{Si}$ CP MAS NMR spectrum of SP34-HCl is further measured (Fig. S5, ESI[†]), revealing that the strong signal should comprise the co-contribution of $\text{Si}(\text{OSi})_2(\text{OAl})_2$ and newly generated defective $\text{Si}(\text{OSi})_m(\text{OAl})_{(3-m)}(\text{OH})$ ($m = 0-2$). The latter should be formed due to the dealumination, for example, the removal of Al from the $\text{Si}(\text{OSi})_1(\text{OAl})_3$ species. The spectrum of SP34-HCl-i presents a considerable change in the Si environments, featuring two broad signals around -99 and -109 ppm. Combined with the $^1\text{H} \rightarrow ^{29}\text{Si}$ CP NMR results (Fig. S5, ESI[†]), the resonances at -91 and -99 ppm should be mainly contributed by hydrolyzed silanols located at the edge of Si islands. And the broad signal at -109 ppm having less connection with hydroxyl arises from amorphous SiO_2 . These results imply that Si islands have good resistance to acid leaching. The ^{31}P and ^{27}Al spectra of the samples are shown in Fig. S6 (ESI[†]). Less pronounced changes can be found for SP34-TEAOH, SP34-HCl and SP34-HCl-i in comparison with those for the precursor. Amorphous SP34-NaOH, however, shows very different P and Al spectra. All P species transform into hydrolyzed $\text{P}(\text{OAl})_x(\text{OH})_y$. For Al atoms, a large amount of octahedral Al species ($\delta = 2$ ppm) appears and coexists with

tetrahedral Al ($\delta = 60$ ppm). The obvious low-field shift of tetrahedral Al confirms that most of the residual Al atoms in SP34-NaOH are situated in aluminosilicate environments.

On the basis of the above characterizations, the relative stability of the local atomic environments in SAPO molecular sieves and the formation of hollow crystals are rationalized as follows. For the alkaline treatment, framework P atoms are the most sensitive to the leaching. Following the extraction of P, Al and Si atoms in the P-rich Al–O–P domains, which are mainly composed of $\text{Al}(\text{OP})_4$ species and isolated $\text{Si}(\text{OAl})_4$ species with P as the second coordination neighbours, will be influenced and removed. Moreover, Si atoms in the $\text{Si}(\text{OSi})_4$ environments are also sensitive to the base etching, though they have better stability than P. Framework Al in the Si–O–Al domains has the best stability in basic media, which can offer super protection to the Si atoms around itself and fabricate robust Si–Al environments to resist the base leaching. Indeed, the inhibition of Si extraction due to high framework Al content has been proven in the aluminosilicate zeolites.⁴ Under extreme conditions using NaOH, framework P atoms and $\text{Si}(\text{OSi})_4$ species will be extensively leached and part of the tetrahedral Al transforms to octahedral following the destructuring. Moreover, abundant $\text{Si}(\text{OSi})_n(\text{OAl})_{(3-n)}(\text{OH})$ ($n = 0, 1$) species located in the residue Si–O–Al domains are created, as indicated by the ^{29}Si NMR. These harsh leaching would cause elemental loss in the order of $\text{P} > \text{Al} > \text{Si}$, and lead to a sharp increase of the Si content in the final product. Given that the precursor SP34-P has a Si-rich external surface, that is, the Si environments become more complex from the core to the shell, more Si islands and Si–O–Al domains are supposed to locate at the outer layer of the crystals. It is thus believed that the abundant and interconnected Si–O–Al domains, which are the most stable environments in the SAPO framework to endure the alkaline treatment,⁸ help the crystal shell keep the integrity and lead to the generation of a hollow morphology, as illustrated in Fig. 3.

In the case of acid treatment, framework Al atoms become the most susceptible one to be attacked and extracted, particularly for the Al atoms in the Al-rich Al–O–P domains. The leaching of Al would cause the corresponding removal of P and Si (mainly $\text{Si}(\text{OAl})_4$ species) located inside the Al–O–P domains. Si atoms in the Si islands have good resistance to acid leaching. It is supposed that Si islands may provide a slight stabilization effect to the Al atoms around themselves, which is somewhat like the protection of Si by Al in the alkaline treatment. Upon intensification of the acid treatment conditions, Al atoms even in proximity to Si islands

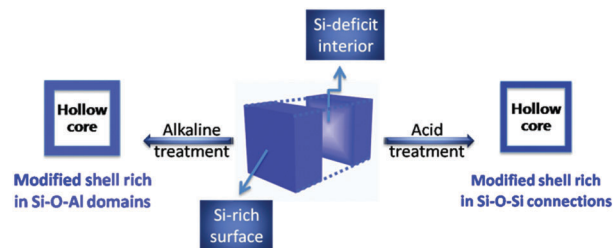


Fig. 3 Formation mechanisms of hollow SAPO-34 single crystals upon acid and alkaline treatments.

may be extracted, generating Si environments that are not fully condensed, among which the highly hydrolyzed Si species (e.g. $\text{Si}(\text{OSi})(\text{OH})_3$) are not stable enough in the acid media and would be further hydrolyzed and removed. On the whole, the acid treatment extracts more Al than P and Si, and leaves Si as the dominant framework T atom. Regarding the formation of hollow crystals, it should once again result from the Si enrichment at the outer shell. The existence of interconnected Si–O–Si networks ($\text{Si}(\text{OAl})_n(\text{OSi})_{(4-n)}$, $n = 0-2$) protects the crystal outer layer from dissolution in the acid media (Fig. 3).

Additionally, high-Si SAPO-20 molecular sieves with surface Si enrichment are synthesized and subjected to the acid/base treatments to further verify the above conclusions about the formation mechanisms of the hollow structure. Detailed information about the samples is given in Table S1, S2 and Fig. S7–S9 (ESI†). Upon TMAOH treatment, a beautiful hollow product with moderate crystallinity can be readily obtained. However, low-crystallinity products with some broken particles seem inevitable for the acid-treated SAPO-20-HCl. From the ^{29}Si spectra (Fig. S9, ESI†) of the samples, SAPO-20 possesses an uncommon ^{29}Si environment with a high concentration of $\text{Si}(\text{OAl})_3$ species. The Si spectra of SAPO-20-TMAOH and SAPO-20-HCl show some similarity to those of SP34-TEAOH and SP34-HCl-i respectively. Basically, the changes of SAPO-20 upon base and acid treatments are well correspondent with the existence of abundant Si–O–Al domains and fewer Si–O–Si connections in the framework. These results are consistent with the above studies on SP34-P and suggest that the preparation of a SAPO precursor with suitable Si coordination environments at the outer layer of crystals is essential in selective etching to achieve a well-preserved hollow product.

The model alkylation reaction of benzene with benzene alcohol (BA) is employed to evaluate the catalytic performance of the hollow-structured SAPO molecular sieves. Because the reagents have larger sizes than the micropores of SAPO-34, the reaction is very susceptible to the external surface area and the accessibility of the acid sites. As shown in Fig. S10 (ESI†), the BA conversion over SP34-HCl is about seven times higher than on SP34-P, though both samples possess similar acid concentration and strength as indicated by NH_3 -TPD (Fig. S11, ESI†). SP34-TEAOH, having a higher acid strength than SP34-P and SP34-HCl, also displays better catalytic activity. The obviously improved catalytic performance observed on the hollow catalysts should be related to the increased external surface area and meso-/macroporous volume.

In summary, hollow SAPO single crystals with a shell thickness of 30–50 nm have been successfully prepared *via* post-synthetic treatment. Si gradients in the crystals have been revealed to play

an important role in the generation of a hollow structure with a Si-rich external surface. For base or acid treatment, the crucial micro-environments for a well preserved crystal shell are the enriched Si–Al domains and Si islands at the outer layers of crystals, respectively. The hollow products show a large external surface area and pore volume, which enhance the catalytic performance and benefit applications as catalyst supports and microreactors (when a nanosized hollow structure is created). We expect that more useful hollow SAPO molecular sieves will be prepared using this facile strategy.

This work was supported by National Natural Science Foundation of China (21476228, 21473182 and 21101150).

Notes and references

- (a) F. Caruso, R. A. Caruso and H. Mohwald, *Science*, 1998, **282**, 1111–1114; (b) J. Hu, M. Chen, X. Fang and L. Wu, *Chem. Soc. Rev.*, 2011, **40**, 5472–5491; (c) Y. Li and J. Shi, *Adv. Mater.*, 2014, **26**, 3176–3205; (d) K. An and T. Hyeon, *Nano Today*, 2009, **4**, 359–373; (e) F. Schuth, *Chem. Mater.*, 2014, **26**, 423–434; (f) V. Valtchev, *Chem. Mater.*, 2002, **14**, 4371–4377.
- (a) X. D. Wang, Y. Tang, Y. J. Wang, Z. Gao, W. L. Yang and S. K. Fu, *Chem. Commun.*, 2000, 2161–2162; (b) S. Li, T. Boucheron, A. Tuel, D. Farrusseng and F. Meunier, *Chem. Commun.*, 2014, **50**, 1824–1826; (c) V. Valtchev, *Chem. Mater.*, 2002, **14**, 956–958.
- (a) L. Han, J. Yao, D. Li, J. Ho, X. Zhang, C. H. Kong, Z. M. Zong, X. Y. Wei and H. Wang, *J. Mater. Chem.*, 2008, **18**, 3337; (b) D. Xi, Q. Sun, J. Xu, M. Cho, H. S. Cho, S. Asahina, Y. Li, F. Deng, O. Terasaki and J. Yu, *J. Mater. Chem. A*, 2014, **2**, 17994–18004.
- J. C. Groen, T. Bach, U. Ziese, A. M. Paulaime-van Donk, K. P. de Jong, J. A. Moulijn and J. Pérez-Ramírez, *J. Am. Chem. Soc.*, 2005, **127**, 10792–10793.
- (a) C. Dai, A. Zhang, L. Li, K. Hou, F. Ding, J. Li, D. Mu, C. Song, M. Liu and X. Guo, *Chem. Mater.*, 2013, **25**, 4197–4205; (b) J. Zhou, Z. Hua, W. Wu, Z. Liu, Y. Zhu, Y. Chen and J. Shi, *Dalton Trans.*, 2011, **40**, 12667–12669.
- (a) Y. Wang, M. Lin and A. Tuel, *Microporous Mesoporous Mater.*, 2007, **102**, 80–85; (b) D. Fodor, L. Pacosova, F. Krumeich and J. A. van Bokhoven, *Chem. Commun.*, 2014, **50**, 76–78.
- (a) A. Corma, *Chem. Rev.*, 1997, **97**, 2373–2419; (b) B. M. Lok, C. A. Messina, R. L. Patton, R. T. Gajek, T. R. Cannan and E. M. Flanigen, *J. Am. Chem. Soc.*, 1984, **106**, 6092–6093; (c) P. Tian, Y. Wei, M. Ye and Z. Liu, *ACS Catal.*, 2015, **5**, 1922–1938.
- D. Verboekend, M. Milina and J. Pérez-Ramírez, *Chem. Mater.*, 2014, **26**, 4552–4562.
- M. Yang, P. Tian, C. Wang, Y. Yuan, Y. Yang, S. Xu, Y. He and Z. Liu, *Chem. Commun.*, 2014, **50**, 1845–1847.
- (a) J. C. Groen, S. Abelló, L. A. Villaescusa and J. Pérez-Ramírez, *Microporous Mesoporous Mater.*, 2008, **114**, 93–102; (b) K. P. de Jong, J. Zecevic, H. Friedrich, P. E. de Jongh, M. Bulut, S. van Donk, R. Kenmogne, A. Finiels, V. Hulea and F. Fajula, *Angew. Chem., Int. Ed. Engl.*, 2010, **49**, 10074–10078.
- S. Abelló, A. Bonilla and J. Pérez-Ramírez, *Appl. Catal., A*, 2009, **364**, 191–198.
- P. Tian, B. Li, S. Xu, X. Su, D. Wang, L. Zhang, D. Fan, Y. Qi and Z. Liu, *J. Phys. Chem. C*, 2013, **117**, 4048–4056.
- H. J. Jung, C. H. Shin and S. B. Hong, *J. Phys. Chem. B*, 2005, **109**, 20847–20853.